Research Article Vol. 29, No. 2 / 18 January 2021 / Optics Express 2855
Optics EXPRESS

EMD and VMD-GWO parallel optimization algorithm to overcome Lidar ranging limitations

BAOLING QI,[1,3] GUOHUI YANG,[2] DONGBING GUO,[1] AND CHUNHUI WANG[1,4]

[1]National Key Laboratory of tunable Laser Technology, Harbin Institute of Technology, Harbin, Heilongjiang 150001, China
[2]School of Electronic and Information Engineering, Harbin Institute of Technology, Harbin, Heilongjiang 150001, China
[3]poling780@163.com
[4]wangch_hit@163.com

Abstract: Pulsed Lidar can obtain rich target information in one pulse, but the echo pulse signal is extremely susceptible to low laser transmitting power and complex target environments, resulting in an amplitude that is too low, which affects detection efficiency and ranging accuracy. In this paper, a variational modal decomposition based on gray wolf optimizer (VMD-GWO) and an empirical mode decomposition (EMD) parallel for denoising and signal enhancement in pulse Lidar is proposed and demonstrated completely. First, the adaptive strategy EMD is used for denoising the signal to obtain effective information. The combination of optimal VMD parameters of quadratic penalty α_v and decomposition mode k was obtained by using the GWO to select the modal component with the smallest center frequency as effective information. Second, EMD and VMD-GWO parallel optimization algorithms are used to reconstruct the signal to obtain denoising and enhanced signals. Finally, a real experiment was carried out with the pulse Lidar ranging equipment. Our method compared with EMD-soft, EMD-VMD,WL-db4//EMD-DT and WL-db4//VMD has achieved greater improvement. When the target distance and the reflectivity of the reflectivity plate are 30 m and 10%, respectively, the peak signal-to-noise ratio (PSNR) of the weak echo signal calculated by our method can reach 11.5284 dB. And when in the dead zone of the system ranging, it is effectively denoising and enhancing the signal.

1. Introduction

Lidar is an active remote sensing technology that combines traditional radar technology and modern laser technology, it has the characteristics of high resolution, superior detection performance, and strong anti-interference ability [1–4]. It is widely used in 3D city modeling and cartography, autonomous driving, target reconstruction and terrain mapping [5–7]. In practical applications, the realization of Lidar detection is interfered by many factors. On the one hand, the intensity of the radar echo signal attenuates drastically with distance. On the other hand, the radiation noise in the atmosphere and the current noise in the detection equipment will interfere with the echo signal [8,9], resulting in the inability to accurately obtain weak echo signals. In the current conventional laser ranging system, accurate echo position detection is the key to ensuring the accuracy of ranging. The peak detection method is usually used to determine the echo position, and the distance information of the target is calculated by combining the pulse time of flight (ToF). In the case of low signal to noise ratio, the measurement accuracy is low, the detection range of Lidar system is difficult to increase [10]. It is a key measure to overcome the limitation of Lidar ranging by seeking an effective method of noise filtering and strengthening weak echo signal to increase the effective information proportion in Lidar echo signal.

In recent years, many researchers have paid attention to the detection and processing of weak echo signals in the environment. Rocadenbosch et al. proposed an algorithm based on Kalman

#415287 https://doi.org/10.1364/OE.415287
Journal © 2021 Received 18 Nov 2020; revised 27 Dec 2020; accepted 4 Jan 2021; published 15 Jan 2021

Optics EXPRESS

filter, using least squares as the best evaluation criterion, but the algorithm will lose accuracy while denoising [11]. Some sparse representation denoising method for Lidar data can efficiently restore the lost information caused by random noise [12–14]. Zhou et al. used the wavelet transform method to decompose the signal into different frequency terms through multiple gradient analysis and time-frequency local features, but the wavelet transform needs to choose different wavelet basis functions and determine the number of decomposition levels according to different problems [15]. Empirical Mode Decomposition (EMD) is a new method for processing non-stationary signals. Chang et al. proposed an EMD-soft algorithm that can effectively suppress noise and improve the signal-to-noise ratio, but there is over-decomposition and the signal amplitude is significantly reduced [16]. Compared with wavelet transform decomposition, EMD does not need to establish any basis function, the influence of the difference of basis function on the decomposition result can be eliminated, and decomposing the signal according to the time characteristics of the data itself. It can reflect the physical meaning of the signal better than other time-frequency analysis methods, but it has the disadvantage of modal aliasing. Variational mode decomposition (VMD), proposed by Dragomiretskiy and Zosso in 2014, is a new adaptive signal decomposition method [17]. VMD has been successfully applied in many fields including mechanical diagnosis, biological science and signal processing. VMD uses the characteristics of its own Wiener filter to overcome modal aliasing, and can combine with EMD algorithms to complement each other. In VMD, two key parameters need to be set: the decomposition mode number k and the quadratic penalty α_v [18]. Generally, they are obtained by the trial-and-error method, and will consume a large amount of computing memory and computing time. Therefore, how to select appropriate parameters has become the limitation of VMD. Li et al. proposed a judgment strategy based on peak search and similarity principles to determine the most suitable decomposition modulus, but did not consider the influence of parameters on the decomposition results [19].

In this paper, an EMD and VMD-GWO parallel optimization algorithm is proposed to overcome Lidar ranging limitations. Based on the theoretical model of pulse Lidar, the adaptive strategy is adopted to obtain the effective information of EMD. Meanwhile, GWO algorithm is adopted to obtain the optimal parameters of VMD for signal processing, and then reconstructed the echo signal after EMD and VMD-GWO processed. In a real environment, preset evaluation indicators and the pulse Lidar ranging system was set up for experiments, which respectively verified that our algorithm can effectively extract and enhance echo signals with different amplitudes at different distances, and could effectively overcome the ranging limitation in the ranging dead zone of the system equipment.

This paper is organized as follows. In section 2, the pulsed Lidar system model and the basic methods are given. The proposed algorithm for signal denoising and enhancement is presented in detail in section 3. In section 4, experiments are conducted on both simulated and real Lidar pulse are given to verify the effectiveness of the proposed algorithm.

2. Pulsed Lidar system and methods

2.1. System model of Pulsed Lidar

The schematic of pulse Lidar system is illustrated in Fig. 1. It is composed of a laser transmit system, a laser optical receiver optics system and a signal processing system. According to the Lidar equation, the trailer of the transmitted pulse can be ignored and its time domain envelope approximates to Gaussian [20]

$$S_{tr}(t) = \sum_{m=1}^{\infty} A_{tr} \exp\left(-4\ln 2\left(\frac{t - mT_R}{\tau_{3dB}}\right)^2\right), \tag{1}$$

Optics EXPRESS

where $S_{tr}(t)$ is the model of transmitting pulse signal at time t, is the A_{tr} amplitude of transmitted pulse signal, τ_{3dB} is the full pulse width corresponding to *3 dB* bandwidth, m is the number of pulse, T_R is the pulse repetition period.

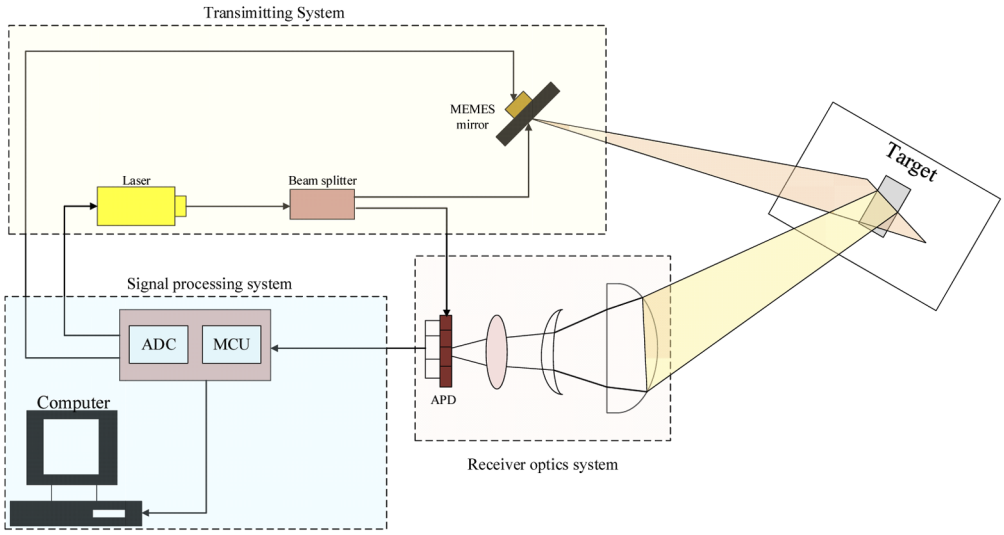

Fig. 1. Schematic diagram of the pulse Lidar system. ADC: analog-digital converter; MCU: microcontroller unit; APD: avalanche photon diode.

The detection of echo pulse signal can be described by Gaussian function

$$S_{ec}(t) = \sum_{m=1}^{\infty} A_{ec} \exp\left(-4\ln 2\left(\frac{t - mT_R - 2R/c}{\tau_{3dB}}\right)^2\right) + N_n, \tag{2}$$

where $S_{ec}(t)$ is the model of echo pulse signal at time t, A_{ec} is the amplitude of echo pulse signal R is the distance between the target and the laser source of Lidar system, c is the speed of light in vacuum, N_n is the random additive noise. In actual measurement, there are some non-ideal factors in the signal, such as atmospheric turbulence and attenuation, background noise, detection noise.

A_{ec} can be described as [21]

$$A_{ec} = \frac{P_{ec}P_{tr}}{T_0}\sqrt{\frac{4\ln 2}{\pi}}, \tag{3}$$

where P_{tr} and P_{ec} are the initial transmitting signal power and echo signal power reflected from the target of the pulse Lidar ranging system respectively, and T_0 is the pulse width of the laser.

It is generally considered that the detection target is a Lambert, and the light power reflected to the unit solid angle within the unit area of the target is uniform, and considering the environmental impact and optical system reception, the echo power received by the receiving system is P_{ec}

$$P_{ec} = \frac{\rho P_{tr}\tau_1^2\tau_2^2 S_a}{\pi R^2}. \tag{4}$$

where τ_1 and τ_2 are the transmittance of the atmospheric and optical systems, respectively, S_a is the entrance pupil area, and ρ is the target reflectance. It can be seen that the received power of the system is inversely proportional to the distance between the target and the laser transmitter. As the distance increases, the received echo signal amplitude A_{ec} also decreases. In order to make the amplitude of echo signal meet the requirements of subsequent effective information

Optics EXPRESS

extraction and ranging algorithms, it is not practical method for the designed Lidar to improve the power of laser transmitter or expand the optical area, especially to improve the power of laser. Therefore, it is urgent to denoising and signal enhancement of weak echo signal under certain power to overcome the application limitation of ranging algorithm.

2.2. Basic theory of EMD

EMD is different from the traditional processing method which takes Fourier transform as the core and requires the assumption that the signal is stationary or piecewise stationary. Instead, it is an adaptive time-frequency analysis method driven by the structural characteristics of the data itself, with good time-frequency resolution and is very suitable for the analysis of nonlinear and non-stationary signals [22]. The overall idea of EMD is to find the instantaneous equilibrium position of the signal to extract a single vibration mode component. Through EMD decomposition, the complex signals can be decomposed into a series of intrinsic modal functions (IMF). The IMFs satisfies the following two conditions:

1) In the entire data range, the number of extreme points and zero points is equal or only one difference.

2) At any point, the average value of the envelope formed by the maximum point and the minimum point is zero.

The adaptive decomposition of non-stationary signals through EMD includes finding all local maxima and local minima of signal $f(t)$, using cubic spline functions to interpolate the maxima and minima, respectively, to obtain the upper envelope $f_{\max}(t)$ and the lower envelope $f_{\min}(t)$ of the signal, and then calculating the mean values of the upper and lower envelopes

$$f_{mean} = \frac{f_{\max}(t) + f_{\min}(t)}{2}, \tag{5}$$

The difference value $h(t)$ can be obtained by subtracting the mean $f_{mean}(t)$ from the original signal $f(t)$

$$h(t) = f(t) - f_{mean}(t), \tag{6}$$

Determine whether the difference $h(t)$ meets the basic conditions of IMF. If it meets the basic conditions, there is $imf_1(t) = h(t)$, the difference will be selected as the first IMF. If not, $h(t)$ will be used as the new original signal to recalculate the difference until the first IMF that meets the basic conditions is obtained, then calculate the remaining component

$$r_1(t) = f(t) - imf_1(t), \tag{7}$$

Then, $r_1(t)$ is substituted into Eqs. (5), (6) and (7) respectively as the new original signal to obtain $imf_2(t), imf_3(t), \cdots, imf_n(t), imf_2(t), imf_3(t), \cdots, imf_n(t)$ in turn. When the remaining component $r_n(t)$ becomes a monotonic function, the decomposition process was stopped. Finally, the original signal $f(t)$ is decomposed by EMD into the sum of n IMFs and a monotonic trend term

$$f(t) = \sum_{i=1}^{n} imf_i(t) + r_n(t). \tag{8}$$

2.3. Brief description of VMD

The VMD algorithm can decompose a signal $f(t)$ into an ensemble of limited bandwidth modal functions, so that the sum of estimated bandwidth of each modal function, the corresponding

Optics EXPRESS

constrained variational model can be expressed as

$$\begin{aligned} &\min_{\{u_k\}\{w_k\}} = \left\{ \sum_k ||\partial_t[(\delta(t) + {}^{j}/_{\pi t}) * u_k(t)]e^{-jw_k t}||_2^2 \right\} \\ &s.t. \sum_k u_k = f(t), \end{aligned} \tag{9}$$

where $\{u_k\} = \{u_1, u_2, \cdots, u_k\}$ is the k modes obtained by decomposition, $\{w_k\} = \{w_1, w_2, \cdots, w_k\}$ is the center frequency of each component, $\partial(t)$ is the gradient with respect to t, * is the convolution, j is the imaginary unit; s.t is the constraint condition, and $\delta(t)$ is the unit pulse function, $f(t)$ is the original signal to be decomposed.

In order to solve the optimal solution of the variation constraint model of VMD, the quadratic penalty factor α_v and Lagrange multiplier $\lambda(t)$ are introduced to transform the above constrained problem into the unconstrained variational problem, as follow

$$\begin{aligned} L(\{u_k\}, \{w_k\}, \lambda) &= \alpha_v \sum_k \left\| \partial_t \left[\left(\delta(t) + \tfrac{j}{\pi t} \right) * u_k(t) \right] e^{-jw_k t} \right\|_2^2 \\ &+ \left\| f(t) - \sum_k u_k(t) \right\|_2^2 + \left\langle \lambda(t), f(t) - \sum_k u_k(t) \right\rangle, \end{aligned} \tag{10}$$

VMD adopts the alternate direction method of multiplication (ADMM) [23] to solve the above variational model, by alternately updating u_k^{n+1}, w_k^{n+1}, λ_k^{n+1} to find the saddle point of the extended Lagrange function, this point is the optimal solution of the variational model . The value problem of u_k^{n+1} can be expressed as

$$u_k^{n+1} = \arg\min_{u_k \in X} \left\{ \begin{array}{l} \alpha_v \left\| \partial_t \left[\left(\delta(t) + \frac{j}{\pi t} \right) * u_k(t) \right] e^{-jw_k t} \right\|_2^2 \\ + \left\| f(t) - \sum_i u_i(t) + \frac{\lambda(t)}{2} \right\|_2^2 \end{array} \right\}. \tag{11}$$

Specific steps are as follows

Step 1. Set $n = 0$ and initialize u_k^{n+1}, w_k^{n+1}, λ_k^{n+1};

Step 2. Execute loop $n = n + 1$, update u_k, w_k for all w>0 components

$$\hat{u}_k^{n+1} = \frac{\hat{f}(w) - \sum_{i \neq k} \hat{u}_i(w) + \frac{\hat{\lambda}(w)}{2}}{1 + 2\alpha(w - w_k)^2}, \tag{12}$$

$$w_k^{n+1} = \frac{\int_0^\infty w|\hat{u}_k(w)|^2 dw}{\int_0^\infty |\hat{u}_k(w)|^2 dw}, \tag{13}$$

Step 3. Then update λ

$$\lambda^{n+1}(w) = \hat{\lambda}^n(w) + \tau \left(\hat{f}(w) - \sum_k \hat{u}_k^{n+1}(w) \right), \tag{14}$$

Step 4. For a given discrimination accuracy e>0, if the following conditions are satisfied, the iteration will be stopped, otherwise return to Step. 2

$$\frac{\sum_k ||\hat{u}_k^{n+1} - \hat{u}_k^n||_2^2}{||\hat{u}_k^n||_2^2} < e. \tag{15}$$

where $\hat{u}_k$ is the frequency spectrum of the mode component, $\hat{f}(w)$ is the signal frequency spectrum, τ is the fidelity of the signal, and n is the number of iterations.

Optics EXPRESS

3. Principle of the proposed algorithm for signal enhancement

3.1. Adaptive strategy to select EMD decomposition parameters

Due to the influence of target's reflection angle, reflectivity, position distance and the radar backscattered, the echo pulse signal will be submerged in the noise [24]. Based on the above analysis on the basic theory of EMD, the pulse signal can be decomposed into a series of IMFs and a trend term by EMD, which is widely used in the extraction and denoising of echo signal. The noise is mainly concentrated in the IMFs of the high-frequency items, if the number of modes selected in the reconstructed signal is too much, the noise elimination is not complete. If there are too few modes, it is easy to cause the loss of useful information. Therefore, how to select effective information items and remove noise items is the key issue.

By calculating the correlation coefficient between the original time domain signal and each IMF component, the correlation and uncorrelated items are distinguished as the boundary between signal and noise.

$$R(f, imf_i) = \frac{\sum_{t=1}^{N} (f(t) - \bar{f})(imf_i(t) - \overline{imf}_i)}{\sqrt{\sum_{t=1}^{N} (f(t) - \bar{f})^2 \sum_{t=1}^{N} (imf_i(t) - \overline{imf}_i)^2}}. \tag{16}$$

where $f(t)$ is the original signal, $\bar{f}$ is the mean of signal, $imf_i(t)$ is the i-th component of IMF, $\overline{imf_i}$ is the mean of the $i-th$ IMF component, N is the length of the signal.

In this paper, we choose the first local maximum in $R(f, imf_i)$ as the dividing line. Before the maximum, the noise is the main section of the IMFs, and the rest is the dominant part of the signal.

3.2. Optimize VMD parameters based on GWO

Grey wolf optimizer is a new swarm intelligence algorithm proposed by Seyedali Mirjalili in 2014 [25]. The algorithm simulates the social hierarchy and hunting behavior of gray wolves, and achieves the purpose of searching for the best through the processes of wolves tracking, encircling prey and hunting. GWO has simple principles, fewer adjustable parameters and strong global search capabilities. The key steps to find the optimal VMD key parameters through GWO are as follows.

(i) Social hierarchy

In the GWO, the social hierarchy is mainly divided into α, β, δ and ω wolves. Among them, the best value of the candidate solution in the gray wolfs is set as the wolf α, the second best value as wolf β, and the third best value as wolf δ, and the remaining candidate solutions are set as wolf ω. In the process of hunting, the position of the wolf is updated according to the rules. At the same time, in the iterative process, the leadership gray wolfs will be replaced by the gray wolf with better adaptability.

(ii) Encircling prey

Grey wolves encircle prey during and need to determine the distance between the individual and the prey. According to the distance, complete the gray wolf position update

$$D = |C \cdot X_p(t) - X(t)|, \tag{17}$$

$$X(t+1) = X_p(t) - A \cdot D. \tag{18}$$

where $X_p(t)$ is the position vector of the prey, $X(t)$ is the position vector of a grey wolf, D is the distance between the gray wolf and prey, and t is the current iteration. So the coefficients A and

Optics EXPRESS

C can be calculated as follows

$$A = 2a \cdot r_1 - a, \tag{19}$$

$$C = 2r_2, \tag{20}$$

where $a = 2 - 2(t/t_{\max})$, where $t_{\max}$ is the maximum number of iterations are linearly decreased from 2 to 0 over the course of iterations and r_1, r_2 are random vectors in [0,1].

(iii) Hunting

When the wolves completes the encirclement of the prey, the wolf α leads the wolf β and the wolf ω to guide the wolves to shrink the encirclement of the prey to achieve the purpose of hunting. The mathematical description is as follows

$$\begin{cases} D_\alpha = |C_1 \cdot X_\alpha - X| \\ D_\beta = |C_2 \cdot X_\beta - X| \\ D_\delta = |C_3 \cdot X_\delta - X| \end{cases}, \tag{21}$$

$$\begin{cases} X_1 = X_\alpha - A_1 \cdot D_\alpha \\ X_2 = X_\beta - A_2 \cdot D_\beta \\ X_3 = X_\delta - A_3 \cdot D_\delta \end{cases}, \tag{22}$$

In this iteration cycle, the final gray wolf position is recorded as

$$X(t+1) = \frac{X_1 + X_2 + X_3}{3}. \tag{23}$$

Where $X_\alpha, X_\beta, X_\delta$ represents the position of wolf α, wolf β and wolf δ, respectively, and X_1, X_2, X_3 represents the step length of the gray wolf individual in the direction of wolf α, wolf β and wolf δ respectively.

To achieve parameter optimization through GWO, it is necessary to determine the fitness function. The energy entropy value reflects the uncertainty and complexity of the signal [26]. The Energy entropy is used to represent the distribution of the signal energy. The high energy entropy and the low energy entropy correspond to the small and significant proportion of the signal in the total energy respectively. The energy entropy values of each mode are calculated by using the VMD model under the positions of the search agents according to the following equation

$$H(u_k) = -P_k \log P_k, \tag{24}$$

where $H(u_k)$ is the energy entropy of component u_k, $P_k = E_k/E$ is the percentage of the energy of the k-th mode in the total signal energy, $E_k = \sum_{t=1}^{N} u_k(t)^2$,and $E = \sum_{i=1}^{k} u_i(t)^2$.

The modal component corresponding to the local minimum of the first energy entropy is taken as the fitness function in the parameter optimization process [27]. It can be described as follows

$$fitness = \min_l H. \tag{25}$$

Through the iterative calculation of the GWO algorithm, the secondary penalty factor α_v and the decomposition level k of the VMD under the optimal fitness value are obtained, and then the VMD components are arranged from low to high center frequency, and we select the component with the smallest center frequency as signal envelope in parallel processing. Record the pseudo code of the GWO algorithm in Algorithm 1.

Optics EXPRESS

Algorithm 1. Pseudocode for GWO

Initialize the grey wolf population position X_i

Initialize a, A and C

Calculate the fitness of each search agent

X_α = the best search agent

X_β = the second best search agent

X_δ = the third best search agent

While (t < maximum iteration number)

for each search agent

Update the position of the current search agent by Equation()

end for

Update a, A and C

Calculate the fitness of all search agents

Update X_α, X_β and X_δ

$t = t + 1$

end while

return $X_\alpha(\alpha_v, k)$

3.3. Procedure of proposed algorithm

Through the EMD of the adaptive strategy we can get the signal $f_1(t)$ after denoising in Section 3.1. At the same time, the original signal is processed in section 3.2. We use the GWO algorithm with energy entropy as the fitness function to obtain the adaptive optimal VMD key parameters, and then the selected signal part was taken as $f_2(t)$. Finally, the denoising and amplitude enhanced pulse signal was obtained by our method.

$$f'(t) = f_1(t) + f_2(t). \tag{26}$$

Figure 2 shows the flowchart of the proposed algorithm. The detailed steps of this algorithm are as follows

Step 1: Input original signal $f(t)$ to adaptive strategy EMD. The signal is decomposed by using EMD, By calculating the adaptive cross-correlation coefficient, the signal components are selected to obtain the reconstructed signal $f_1(t)$.

Step 2: Input original signal $f(t)$ to VMD-GWO. The ranges of VMD parameters to be optimized are set and the GWO model is initialized, including the number of search agent and the maximum iteration number. We takes k to an integer in the interval (2,10), α_v in the interval (1400,10000), the number of search agents is 30, and the maximum iterations is 15.

Step 3: Signal decomposed by VMD, calculate the fitness value of each search point and save the smallest fitness value during each iteration.

Step 4: Iteratively find the optimal parameters until the maximum number of iterations is reached. By judging the conditions, until the maximum number of iterations is reached, the optimized parameters and the best fitness value are saved.

Optics EXPRESS

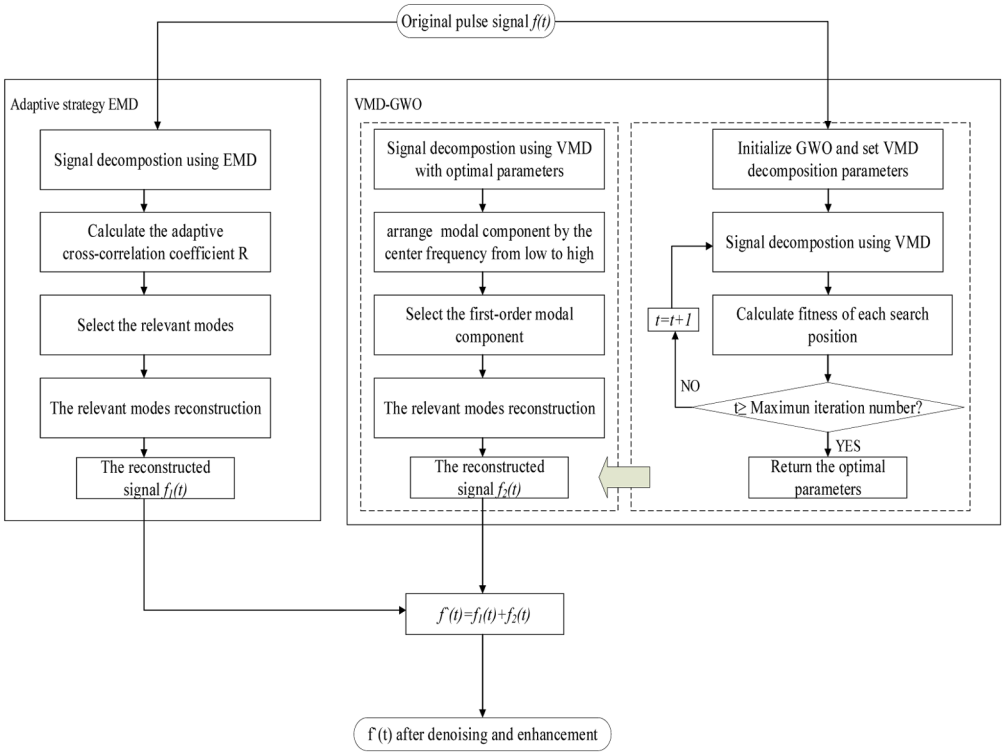

Fig. 2. Flow chart of the proposed algorithm

Step 5: The signal is decomposed by the VMD substituted into the optimized parameters. Then the modal components after VMD decomposition are arranged from low to high center frequency, and the first-order component is selected, and the reconstructed signal is $f_2(t)$.

Step 6: The signal processed by the parallel algorithm is reconstructed. The denoising and enhanced pulse signal is obtained through $f'(t) = f_1(t) + f_2(t)$ for further signal processing.

4. Results of experiment and simulation

4.1. Evaluation index

We need to verify that the range finding limitation that our algorithm overcomes mainly has three aspects: 1) The echo signal is weak, which results in limited range. 2) At the same time of denoising, the amplitude of the signal is also reduced correspondingly and the useful information is less contained. 3) Because the pulse Lidar ranging system has the shortcoming that the detector is easily saturated or damaged, there is a ranging dead zone.

In order to evaluate and compare the performance of the proposed method and other signal processed methods, the evaluation indexes are set as the output peak signal-to-noise ratio ($PSNR_{out}$) and the peak timing error (PTE).

$$PSNR_{out} = 10 \cdot \log 10 \left(\frac{MAX^2}{\frac{1}{N} \sum_{t=1}^{N} (f(t) - f'(t))^2} \right), \tag{27}$$

$$PTE = |t_{ec} - t'_{ec}|. \tag{28}$$

Optics EXPRESS

where MAX is the maximum amplitude of the reconstructed signal, $f(t)$ is the original signal, $f'(t)$ is the denoising signal, N is the length of the signal, t_{ec} is the actual echo timing, and t'_{ec} is the peak echo timing detected by the algorithm.

In this paper, our method compare with EMD-soft, EMD-VMD, WL-db4//VMD and WL-db4//EMD-DT algorithms for different evaluation indexes. When the value of PTE is in the range of $3ns$, it means that the current ranging algorithm is successfully detected. After repeated tests, the detection success rate (DSR) can be calculated, and its value reflects whether the distance limit of ranging has been overcome. After processing by different algorithms, the value of $PSNR_{out}$ can effectively evaluate the degree of effective information in the echo signal.

4.2. Experiments and simulated analysis

In order to further illustrate the correctness of $f'(t) = f_1(t) + f_2(t)$, the echo pulse of a reflector with a reflectivity of 35% at a distance of 20 m was obtained by the experimental equipment in Fig. 6. $PSNR_{out}$ and root mean square error $(RMSE)$ under different weight coefficients $rc = f_2(t)/f_1(t)$ were calculated respectively, and the experimental results were recorded as shown in Fig. 3. We can find that when $rc = 1$, the $PSNR_{out}$ has the maximum value and the $RMSE$ is the minimum, so it is a good illustration of the correctness of Eq. (26).

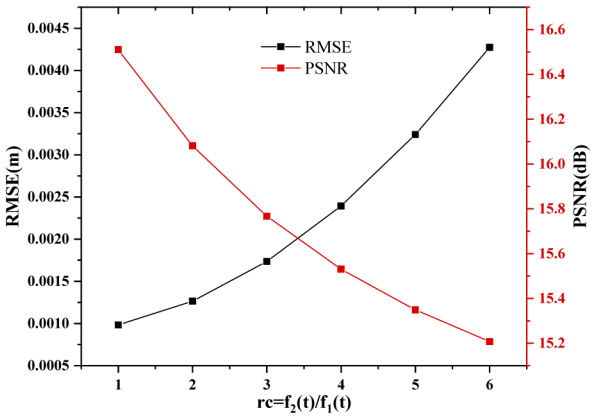

Fig. 3. The result diagram of different weight coefficients

The GWO is newly developed, swarm intelligence optimization algorithm. Compared with artificial fish swarm algorithm (AFSA) and particle swarm optimization (PSO), GWO has better global optimization ability and fewer setting parameters.

In order to make an intuitive illustration, a comparison simulation between GWO and AFSA and PSO is conducted. The standard base function Eason in Eq. (29) which is similar to the pulse model in this paper, is adopted as the test function. Its extreme point is $f(\pi, \pi) = 0$, the maximum number of iterations is 100, the initial population number of artificial fish swarm algorithm and PSO is set as 200, and the congestion factor of AFSA is 0.2. The convergence characteristic diagram obtained through the test function is shown in Fig. 4. It can be seen that GWO algorithm has better applicability in VMD parameter optimization.

$$Eason : f(x) = -\cos(x_1)\cos(x_2)\exp(-((x_1 - \pi)^2 + (x_2 - \pi)^2)) + 1. \tag{29}$$

The laser pulse signal model as an echo pulse signal, simulation experiments are carried out to verify the effectiveness of the proposed method. The synthetic signal consists of an ideal echo pulse supplemented with white Gaussian noise, is shown in Fig. 5, where $SNR_{in} = 5$ dB, the sampling frequency is 5 GHz, transmitted pulse width with 3 dB is 4 ns, pulse repetition

Optics EXPRESS

frequency is 200 kHz and the distance to the target is 50 m. The red line is the ideal echo pulse, and the green line represent the noise signals. We compared the performance of our method with that of different denoising methods, namely, Daubechies4 mother wavelets and VMD parallel optimization algorithm (WL-db4//VMD), EMD with soft thresholding (EMD-soft), VMD method based on EMD (EMD-VMD), and daubechies4 mother wavelets and EMD direct thresholding parallel optimization algorithm (WL-db4//EMD-DT).

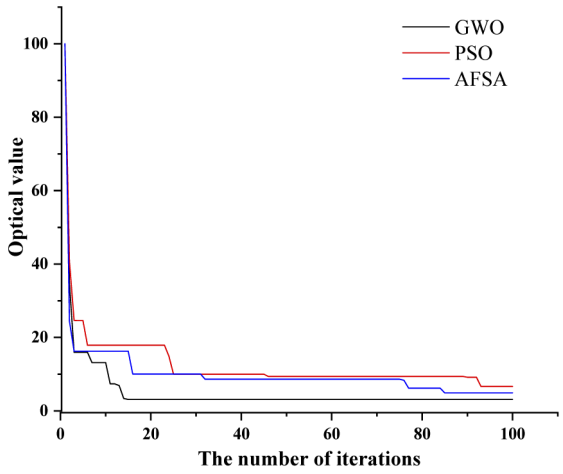

Fig. 4. Comparison of convergence characteristics

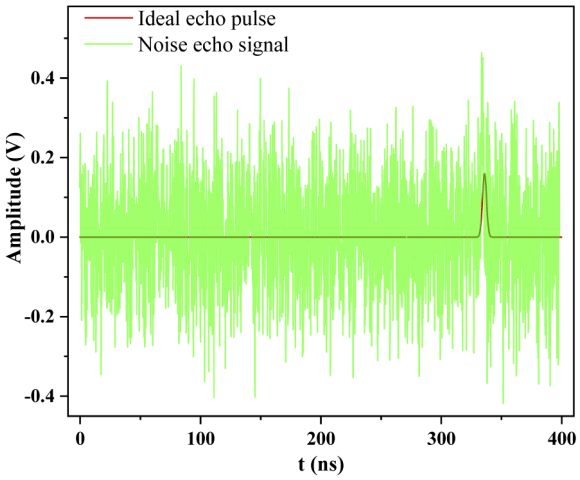

Fig. 5. Ideal echo pulse signal and noise

By processing the noise echo pulse, the experimental result is shown in Fig. 6. As shown in this figure, although the peak value of the denoising signals of WL-db4 //VMD and WL-db4 //EMD-DT is slightly larger than that of our method, the amplitude of the noise is also significantly enhanced. Our method has the highest $PSNR_{out}$ and can enhance the signal well. Therefore, our method has advantages in the processing of pulse signal. But the noise is complex rather than single, so the following is necessary for the processing of Lidar pulse signal in the actual environment.

Optics EXPRESS

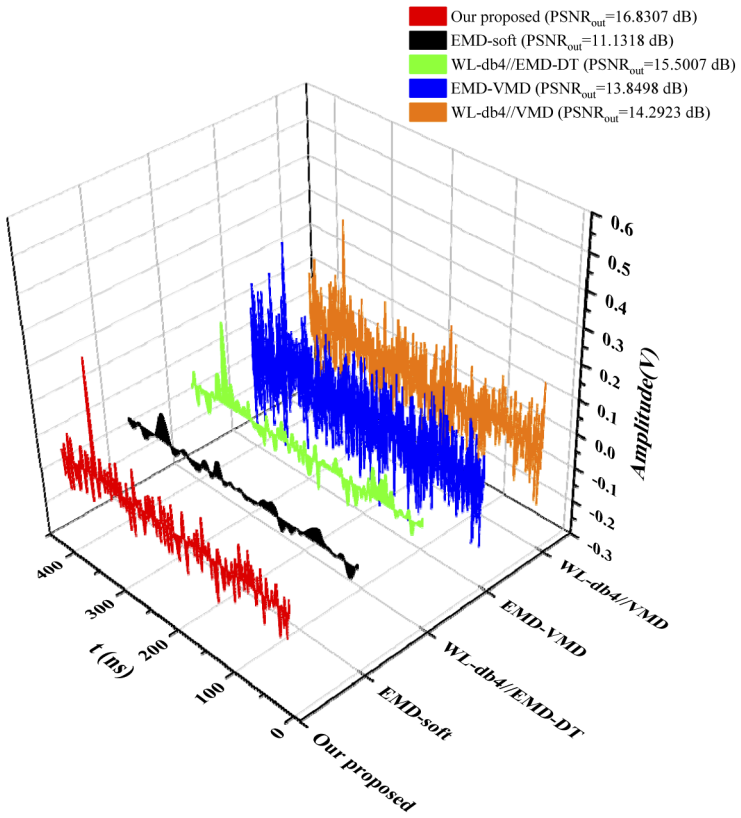

Fig. 6. Comparisons of different signal processing methods for the noisy echo pulse.

4.3. *Experimental system equipment and parameters*

In order to prove the feasibility of our method, we designed the pulsed Lidar ranging system, which is mainly divided into three main parts, including the transmitting system, the receiving system and the signal processing system. The target is the different reflectivity plates at different distances which is calibrated by BOSCH GLM500 laser rangefinder. The experimental equipment and environment are shown in Fig. 7. Table 1 lists the parameters of our experimental system.

Table 1. Specifications of the Lidar system

Parameter	value
Laser wavelength	1064 nm
Pulse width	4 ns
Model of APD	PDB430C
APD response frequency band	250 MHz
Spectral response frequency band	600 to 1150 nm
Size of APD photosensitive surface	3 mm
Receiving system optical aperture	50 mm
ADC sampling rate	5 GSa/s
ADC bandwidth	1 GHz

Optics EXPRESS

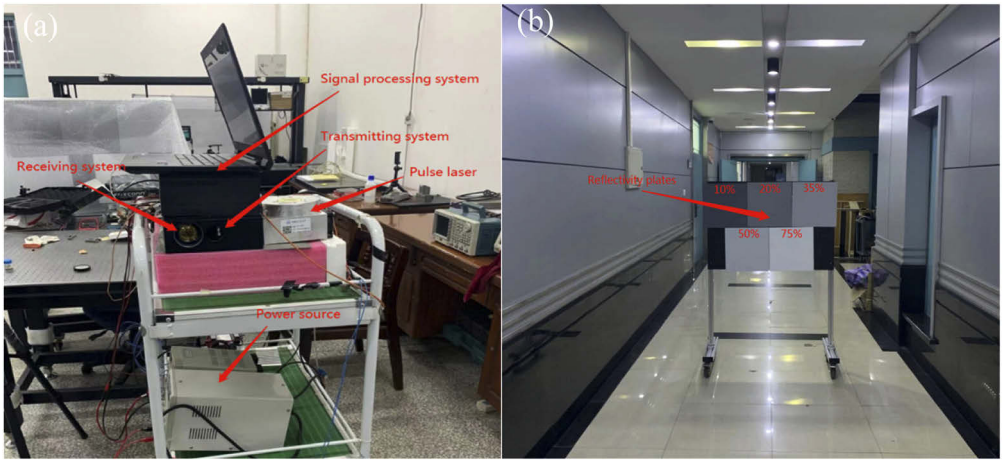

Fig. 7. Experimental system and environment. (a) experimental system and (b) experimental environment

4.4. Experiments on a Pulse Lidar echo signal

In order to verify the echo signal processing performance of the algorithm, the experimental test was carried out on the actual pulse Lidar ranging system. Under low transmitting power, it can simulate the complex ranging environment, so that the echo cannot be directly used for ranging and signal extraction without signal processing. The initial $PSNR_{out}$ under the 10% reflectivity plate is 8.5157 dB at 20 m and 4.5871 dB at 30 m. The advantage is that we can achieve the same effect of signal attenuation due to long distance under standard distance. Under the distance 20 m, 30 m calibrated by the laser rangefinder, the echo signals under different standard reflectance plates were processed respectively, and the $PSNR_{out}$ was calculated and record the result in Table 2. And the original return pulse and the pulse signal processed by the corresponding algorithm under the corresponding distance reflectance plate of 10% are shown in Fig. 8 and Fig. 9.

Table 2. $PSNR_{out}$ of the processed echo signal

$PSNR_{out}$(dB)		EMD-soft	EMD-VMD	WL-db4//VMD	WL-db4//EMD-DT	Our proposed
20m	10%	11.1144	9.3605	12.0997	13.4043	14.2221
	20%	12.5658	9.9715	12.4848	13.8083	14.6468
	35%	14.2911	11.2194	14.6187	14.4096	17.3391
	50%	14.8084	12.0963	15.4265	14.6311	17.9380
	75%	15.0137	16.7724	18.3637	18.2424	18.9910
30m	10%	7.0593	5.4241	8.5364	7.7715	11.5284
	20%	8.2853	6.0203	9.8756	8.2651	12.8139
	35%	9.2415	7.9776	10.2450	10.9400	13.0203
	50%	9.7108	8.14221	11.7892	11.1566	13.2705
	75%	10.1883	8.2581	12.7014	12.3768	13.4666

As can be seen from the data in Table 2 the intensity of the echo signal decreases as the reflectivity decreases at different distances. Our proposed algorithm compared with other algorithm has a higher $PSNR_{out}$. When the target distance is 30 m and the reflectivity plate is 10%, $PSNR_{out}$ can reach 11.5284 dB means that the echo pulse signal processed by our proposed

Optics EXPRESS

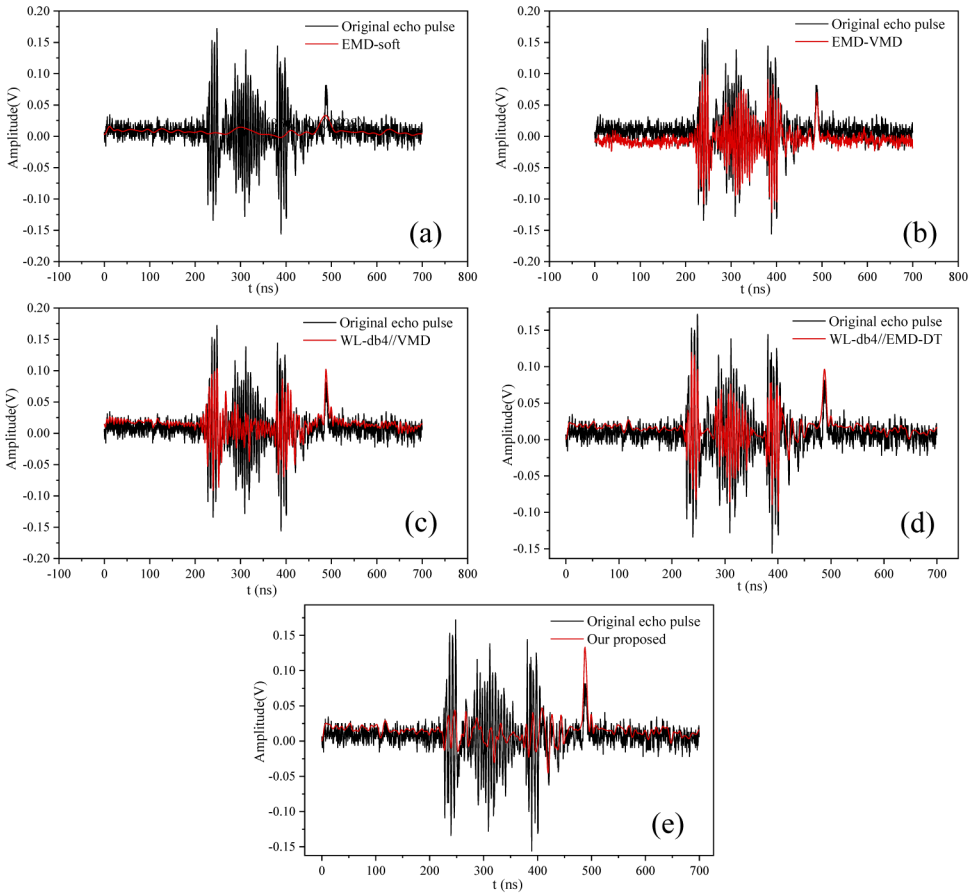

Fig. 8. Echo signals before and after processing at a distance of 20 m. (a) EMD-soft, (b) EMD-VMD, (c) WL-db4//VMD, (d) WL-db4//EMD-DT and (e) Our proposed

algorithm contains the most effective information and the most abundant effective waveform information, which can be better used for further pulse signal processing. The echo pulse signals before and after signal processing under 10% reflectivity plate and at different target distances are recorded in Fig. 8 and Fig. 9 respectively. As can be seen from the figures, our method can enhance the amplitude of echo signal on the basis of denoising, making the amplitude of signal significantly higher than the noise.

To further illustrate the performance of the proposed algorithm for pulse ranging after processing, then we use peak ranging to calculate *PTE* to obtain *DSR*. Most ranging algorithms, including waveform centroid algorithm, constant fraction timing and other algorithms, need to rely on peak values to select calculation points. Therefore, the success rate of peak ranging directly reflects the applicability of the ranging algorithm to echo signals. Table 3 shows the success rate of ranging under different distances and different reflectivity plates.

As shown in Table 3, although the EMD-soft algorithm can remove noise so that the signal peak is larger than the noise amplitude and can be extracted, the processed signal has a large distortion drift, resulting in *PTE* greater than 3 ns. In the weak echo signal at low reflectivity, the echo signal processed by EMD-VMD, WL-db4//VMD and WL-db4//EMD-DT has a peak value smaller than the noise amplitude, which results in the ranging algorithm cannot detect the peak value and the ranging success rate is very low. Our proposed algorithm can effectively detect the

Optics EXPRESS

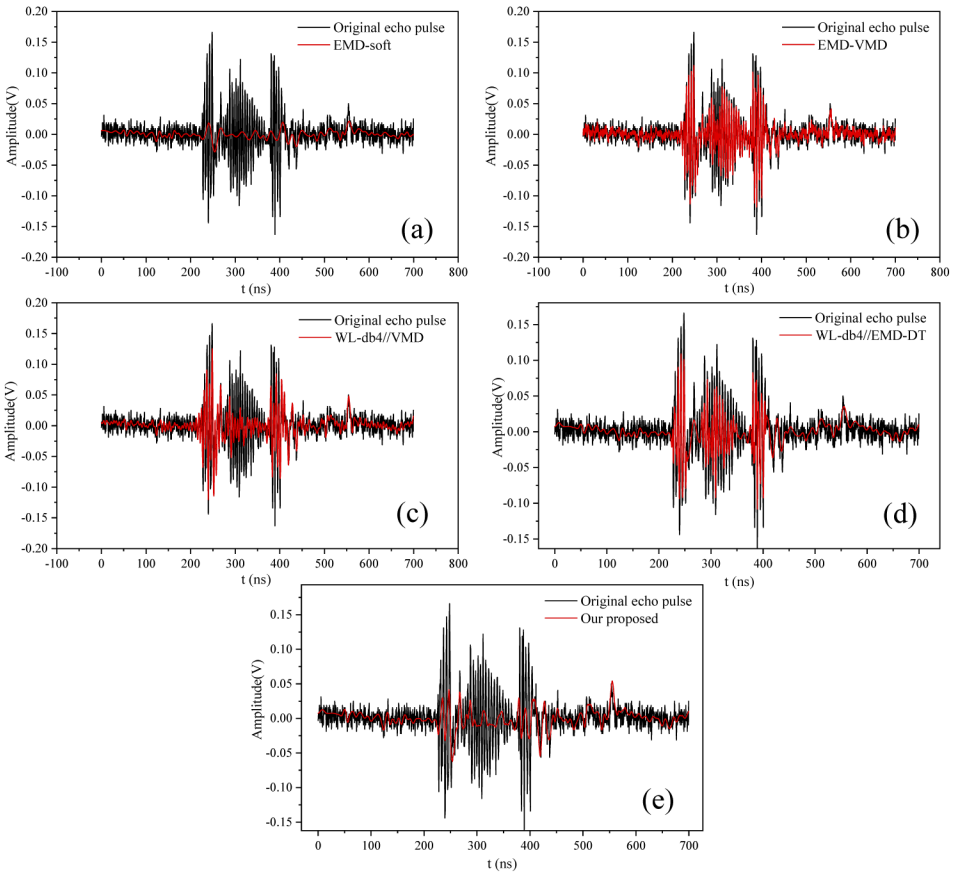

Fig. 9. Echo signals before and after processing at a distance of 30 m. (a) EMD-soft, (b) EMD-VMD, (c) WL-db4//VMD, (d) WL-db4//EMD-DT and (e) Our proposed

Table 3. DSR of the processed echo signal

	DSR(%)	EMD-soft	EMD-VMD	WL-db4//VMD	WL-db4//EMD-DT	Our proposed
20m	10%	30	5	6	8	95
	20%	60	7	9	10	97
	35%	75	10	20	15	100
	50%	90	60	70	60	100
	75%	98	100	100	100	100
30m	10%	10	2	3	5	90
	20%	50	4	7	6	95
	35%	70	6	15	10	98
	50%	85	50	60	40	100
	75%	91	99	99	96	100

peak value under different emission pulse conditions. Even under a 10% reflectivity plate, *DSR* can reach 90%, which has a high ranging success rate.

As can be seen from *DSR* value in Table 3, when the reflectivity plate is 10%, the success rate of our method is greatly improved compared with other methods under the low echo power,

Optics EXPRESS

Table 4. The calculation cost of different algorithms under 10% reflectivity plate

	EMD-soft	EMD-VMD	WL-db4//VMD	WL-db4//EMD-DT	Our proposed
20 m	0.2674 s	0.6935 s	0.6854 s	0.3738 s	0.6516 s
30 m	0.2453 s	0.6309 s	0.5801 s	0.3304 s	0.5732 s

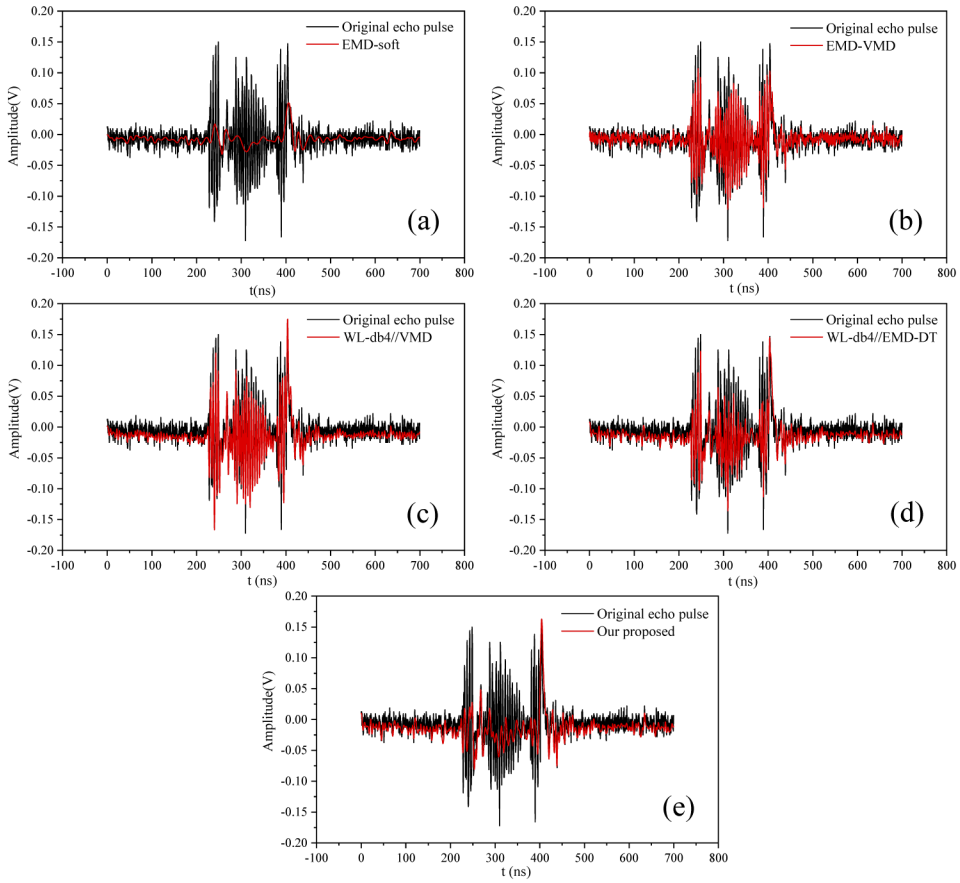

Fig. 10. Echo signals before and after processing at a distance of 7 m. (a) EMD-soft, (b) EMD-VMD, (c) WL-db4//VMD, (d) WL-db4//EMD-DT and (e) Our proposed

that is. However, in the actual experiments, the iterative selection of VMD parameters by GWO is only carried out in the initial measurement of changing environmental targets, so the signal component selection only needs to be carried out by using our method at the same distance. Under the target of 10% reflectivity plate, the calculation cost at different distances is shown in Table 4. It can be seen that EMD-Soft has the lowest computing cost, but compared with EMD-Soft, our DSR improves more than three times, and the detection error has a greater adverse effect than the calculation cost in the field of ranging. Therefore, our method is practical, and with the improvement of hardware processor level, the real-time performance of the system can be further improved by increasing ADC sampling rate.

The pulse ranging Lidar system has the defect that the sensor is easily saturated or damaged. The usual measures are to limit the distance so that there is no target at close range, or to reduce the transmission power. The method in this paper can extract the signal from the submerged noise under the set initial power without changing the system power again. We will carry out

Optics EXPRESS

ranging in the dead zone of the Lidar system, and set a target reflectivity plate of 10% to measure the echo pulse signal at a distance of 7 m and 3 m respectively. In Fig. 10 and Fig. 11 is the echo pulse signal before and after processing.

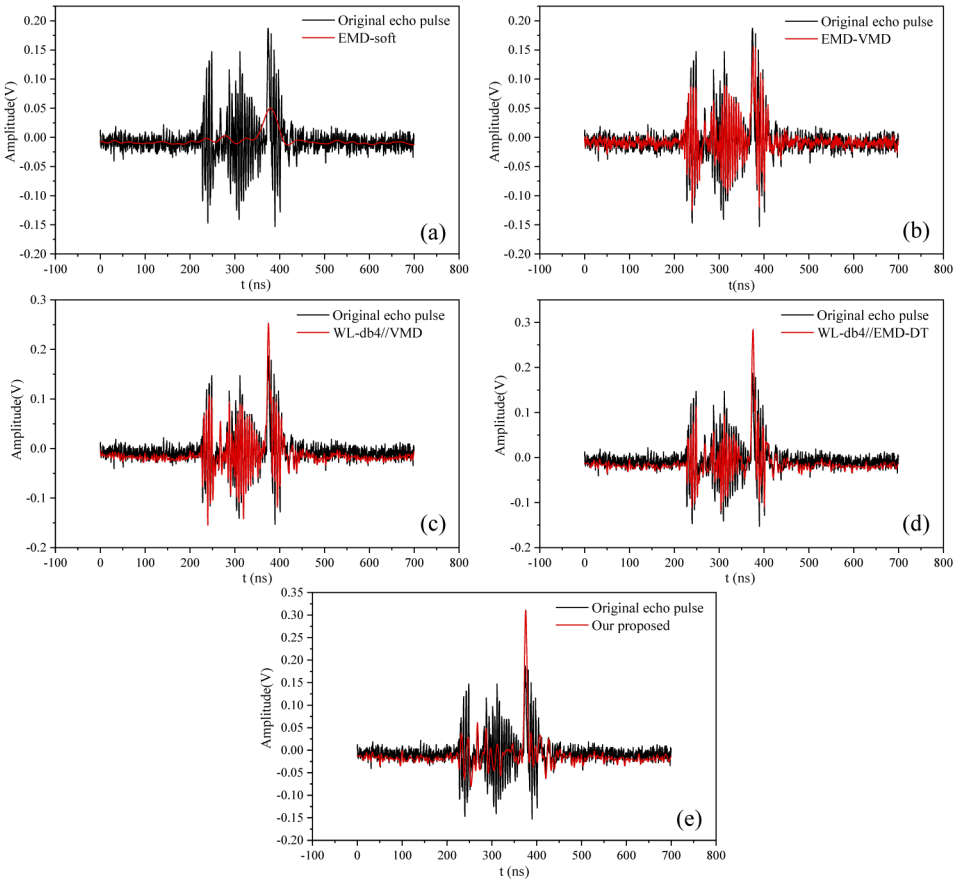

Fig. 11. Echo signals before and after processing at a distance of 3 m. (a) EMD-soft, (b) EMD-VMD, (c) WL-db4//VMD, (d) WL-db4//EMD-DT and (e) Our proposed

As shown in Figs. 10 and 11, the echo signal is completely submerged in noise no matter at a distance of 7 m or 3 m. Even within the internal noise range of the ranging system, the peak value of the echo signal can be significantly higher than the noise, and the noise can be well suppressed. Therefore, under safe power, it is not necessary to consider the limit of saturation or damage of the detector, and can be detected close targets.

5. Conclusion

In this study, a signal denoising and enhancement algorithm of EMD and VMD-GWO parallel optimization was proposed and effective applied in the pulse Lidar ranging system. First, the adaptive cross-correlation function is used to distinguish the EMD signal and noise, and the reconstructed effective signal is obtained. And then, the VMD for signal processing, the decomposition mode number k and quadratic penalty α_v need to be selected appropriately. Therefor the GWO was used to search for the optimal parameters (k, α_v). Then, the VMD-GWO method decomposes the echo signal, which is select the modal component with the smallest center frequency as effective information. Secondly, reconstruct the signals processed simultaneously

Optics EXPRESS

by EMD and VMD-GWO to obtain echo signals. Finally, based on the pulsed Lidar ranging system, different standard reflectors board are used at different distances to simulate low-power echo signals of different amplitudes. When the target distance is 30 m, under the 10% standard reflectance board, the $PSNR_{out}$ of the parallel algorithm in this paper reaches 11.5284 dB, which is 2.6 times higher than the 4.5871 dB of the initial echo signal. And within the range of internal noise, it can also effectively denoising and enhance the signal, which verifies the effectiveness and feasibility of the algorithm. In the next step, we consider using it in the Lidar 3D point cloud scanning system to process the point cloud data to test its performance. In further applications, there may be a lack of real-time performance for our method. Therefore, the judgment of reducing iteration for hardware processing system design and similar environment can be considered to further optimize the algorithm.

Funding. National Key Scientific Instrument and Equipment Development Projects of China (62027823); National Natural Science Foundation of China (61775048); Shenzhen Fundamental Research Program (JCYJ2020109150808037).

Disclosures. The authors declare no conflicts of interest.

References

1. S. Budzan and J. Kasprzyk, "Fusion of 3D laser scanner and depth images for obstacle recognition in mobile applications," Opt. Lasers Eng. **77**, 230–240 (2016).
2. W. Li, Z. Niu, G. Sun, S. Gao, and M. Q. Wu, "Deriving backscatter reflective factors from 32-channel full-waveform LiDAR data for the estimation of leaf biochemical contents," Opt. Express **24**(5), 4771–4785 (2016).
3. W. Xia, S. Han, J. Cao, and H. Y. Yu, "Target recognition of log-polar ladar range images using moment invariants," Opt. Lasers Eng. **88**, 301–312 (2017).
4. K. M. Jakubowski, Q. H. Guo, and M. Kelly, "Tradeoffs between lidar pulse density and forest measurement accuracy," Remote Sens. Environ. **130**(15), 245–253 (2013).
5. J. Q. Wu, Y. Tian, H. Xu, R. Yue, A. Wang, and X. G. Song, "Automatic ground points filtering of roadside LiDAR data using a channel-based filtering algorithm," Opt. Laser Technol. **115**, 374–383 (2019).
6. X. Liang, R. L. Wang, B. Dai, Y. Q. Fang, D. X. Liu, and T. Wu, "Hybrid conditional random field based camera-LIDAR fusion for road detection," Inf. Sci. **432**, 543–558 (2018).
7. J. Heo, S. Jeong, H. K. Park, J. Jung, S. Han, S. C. Hong, and H. G. Sohn, "Productive high-complexity 3D city modeling with point clouds collected from terrestrial LiDAR," Comput. Environ. Urban Syst. **41**, 26–38 (2013).
8. H. J. Jiang, J. C. Lai, W. Yan, C. Y. Wang, and Z. H. Li, "Theoretical distribution of range data obtained by laser radar and its applications," Opt. Laser Technol. **45**, 278–284 (2013).
9. A. I. Nadeev, I. E. Penner, and E. S. Shevtsov, "Photodetector Module for Recording Lidar Signals in the Near-Infrared Region," Atmos. Oceanic Opt. **33**(4), 400–405 (2020).
10. T. A. Teo and W. Y. Yeh, "The Benefit of the Geospatial-Related Waveforms Analysis to Extract Weak Laser Pulses," Remote Sens. **10**(7), 1141 (2018).
11. F. Rocadenbosch, C. Soriano, A. Comeron, and J. M. Baldasano, "Lidar inversion of atmospheric backscatter and extinction-to-backscatter ratios by use of a Kalman filter," Appl. Opt. **38**(15), 3175–3189 (1999).
12. Z. M. Cao and Y. F. Gu, "Sparse Representation Denoising Framework for 3-D Building Reconstruction From Airborne LiDAR Data," IEEE J. Sel. Top. Appl. Earth Observ. Remote Sens. **9**(5), 1888–1900 (2016).
13. Z. Gao and H. Ji, "Transform Learning Based Sparse Coding for LiDAR Data Denoising," IEEE Signal Process. Lett. **26**(3), 480–484 (2019).
14. X. H. Li, H. F. Shen, L. P. Zhang, H. Y. Zhang, Q. Q. Yuan, and G. Yang, "Recovering Quantitative Remote Sensing ProductsContaminated by Thick Clouds and Shadows Using Multitemporal Dictionary Learning," IEEE Trans. Geosci. Electron. **52**(11), 7086–7098 (2014).
15. Z. R. Zhou, D. X. Hua, Y. F. Wang, Q. Yan, S. C. Li, Y. Li, and H. W. Wang, "Improvement of the signal to noise ratio of Lidar echo signal based on wavelet de-noising technique," Opt. Lasers Eng. **51**(8), 961–966 (2013).
16. J. H. Chang, L. Y. Zhu, H. X. Li, F. Xu, B. Liu, and Z. B. Yang, "Noise reduction in Lidar signal using correlation-based EMD combined with soft thresholding and roughness penalty," Opt. Commun. **407**, 290–295 (2018).
17. K. Dragomiretskiy and D. Zosso, "Variational Mode Decomposition," IEEE Trans. Signal Process. **62**(3), 531–544 (2014).
18. C. C. Yi, Y. Lv, and Z. Dang, "A Fault Diagnosis Scheme for Rolling Bearing Based on Particle Swarm Optimization in Variational Mode Decomposition," Shock Vib. **2016**(2), 1–10 (2016).
19. Z. P. Li, J. L. Chen, Y. Y. Zi, and J. Pan, "Independence-oriented VMD to identify fault feature for wheel set bearing fault diagnosis of high speed locomotive," Mech. Syst. Signal Process. **85**(15), 512–529 (2017).
20. Y. X. Li, T. X. Cui, Q. Y. Li, B. Zhang, Y. R. Bai, and C. H. Wang, "Waveform centroid discrimination of return pulse weighting method in LIDAR system," Optik **180**, 840–846 (2019).
21. H. Abdallah, N. Baghdadi, J. S. Bailly, Y. Pastol, and F. Fabre, "Wa-LiD: A new LiDAR simulator for waters," IEEE Geosci. Remote Sens. Lett. **9**(4), 744–748 (2012).

Optics EXPRESS

22. Z. H. Wu, N. E. Huang, S. R. Long, and C. K. Peng, "On the trend, detrending, and variability of nonlinear and nonstationary time series," Proc. Natl. Acad. Sci. U. S. A. **104**(38), 14889–14894 (2007).
23. W. Shi, Q. Ling, K. Yuan, G. Wu, and W. T. Yin, "On the Linear Convergence of the ADMM in Decentralized Consensus Optimization," IEEE Trans. Signal Process. **62**(7), 1750–1761 (2014).
24. K. M. Chang, "Arrhythmia ECG Noise Reduction by Ensemble Empirical Mode Decomposition," Sensors **10**(6), 6063–6080 (2010).
25. S. Mirjalili, S. M. Mirjalili, and A. Lewis, "Grey Wolf Optimizer," Adv. Eng. Softw. **69**, 46–61 (2014).
26. X. J. Chen, Y. M. Yang, Z. X. Cui, and J. Shen, "Vibration fault diagnosis of wind turbines based on variational mode decomposition and energy entropy," Energy **174**(1), 1100–1109 (2019).
27. K. Li, L. Su, J. J. Wu, H. Q. Wang, and P. Chen, "A Rolling Bearing Fault Diagnosis Method Based on Variational Mode Decomposition and an Improved Kernel Extreme Learning Machine," Appl. Sci. **7**(10), 1004 (2017).